Facile access to furo[2',3':4,5]pyrido[3,2,1-*jk*]carbazol-5-ones as blue emitters: photophysical, electrochemical, thermal and DFT studies

Monika Ahuja,[b] Supriya Das[c], Pratibha Sharma,[b] Ashok Kumar,[b] Anvita Srivastava[d], Sampak Samanta[*,a]

[a]Indian Institute of Technology Indore, Department of Chemistry, 453552, Indore, India.

[b]School of Chemical Sciences, Devi Ahilya Vishwavidyalaya, Takshashila Campus, Indore, 452001, India.

[c]Indian Institute of Technology Guwahati, Guwahati, Assam, India.

[d]Nanhi Pari Seemant Engineering Institute Pithoragarh, 262501, India

*Corresponding author: Email:sampaks@iiti.ac.in; Phone: 91-731-2438753

Abstract:

A series of thermally stable (up to ≤339 °C) and blue fluorescent furo[2',3':4,5]pyrido[3,2,1-jk]carbazol-5-ones (FPCOs) with high quantum yields (Ø ≥ 0.75) are reported. The above building blocks were made from a family of Morita-Baylis-Hillman acetate of nitroalkenes and 4-hydroxy-6*H*-pyrido[3,2,1-jk]carbazol-6-one (HPCO) in the presence of DABCO as an organobase at room temperature. All the new chemical structures were assigned by their spectroscopic techniques such as FT-IR, ^{1}H NMR and ^{13}C NMR, HRMS. The solvatochromic studies of prepared scaffolds exhibited blue shifts in absorption and emission spectra with increasing the polarity of solvents. Interestingly, higher quantum yields were also obtained in case of low polar solvents as well as products containing electron-donating groups. The density functional theory calculations indicated that electron-donating substituents led to the lower HOMO-LUMO gap, resulting in bathochromic shifts in absorption spectra. Moreover, chemical hardness, global softness and chemical potential descriptors of compounds are well-estimated. The nature of electronic transition of synthesized scaffolds was well addressed by TD-DFT calculations. In addition, by using NBO and surface analysis calculations, the most nucleophilic and electrophilic sites of title scaffolds were assigned. Interestingly, the cyclic voltammograms of all the FCPOs were shown only one irreversible reduction peak values (-0.62 V to -0.73 V). Therefore, promising charge carrier properties, good thermal robustness and electrochemical stability would make them potential candidates for electronic devices.

1. Introduction

The efficient construction of new π-conjugated donor-acceptor organic materials allegedly called push-pull chromophores, have attracted intense interest in view of their potential applications in multifaceted areas such as analytical sciences, chemiluminescence, fluorescence technology, optoelectronic devices, organic solar cells etc.[1-3]Therefore, the fusion of donor and acceptor scaffolds into one entity is one of the most efficient approaches to create fluorophorically exciting hybrid frameworks. [2]During the past decade, furan moiety has emerged as an electron donating heteroaromatic unit appropriate for the construction of push-pull architectures accompanied with potential applications in the field of optoelectronics and fluorophoric organic materials.[3-4] On the other hand, among fused carbazoles,[5] pyridocarbozolone (PCO) scaffolds are well-known benchmark materials showcasing strong absorption and emission properties.[6] Eventually, they have potential applications in blue-light emitters and organic electroluminescent devices.[6-7]In this context, Kang et al. synthesized an interesting class of 4-hydroxy-5-phenyl-6*H*-pyrido[3,2,1-*jk*]carbazol-6-one derivatives that displayed blue luminescence with moderate quantum yields.[7] We also reported a solvent-free synthesis of pyrano-fused pyridocarbazolones as blue fluorescence emitters.[8]Thus, it would be interesting idea to construct an unprecedented class of donor-acceptor skeleton consisting of PCO and furan units amalgamated in a fused π-conjugated manner that may enhance the fluorescence properties. Towards their efficient access, we envisage that furan moiety could install on PCO skeleton via a domino reaction of MBH acetate of nitroalkene as an ideal 1,3-bielectrophile with enolizable ketone like HPCO in the presence of base.[9] Our on-going research is directed towards the development of new synthetic methods for the synthesis of biologically active fused indoles[10] and their applications in fluorescence materials.[11] Herein, we wish to report further a mild, organobase promoted one-pot approach to FPCOs as blue emitters under mild conditions. In addition, the detailed   photophysical, electrochemical,

thermogravimetric analysis and theoretical insights of the aforesaid molecular structures are reported.

2. Experimental section

2.1 General information:

All the nitro allylic acetates **(2a-h)**[12]and carbazole **1**[13] were synthesized by literature known procedures. All the chemicals were purchased from commercial sources (Sigma Aldrich). All the reactions were carried out either under inert atmosphere or in air and monitored by TLC using Merck 60 F_{254} precoated silica gel plates, and the products were visualized by UV detection. FT-IR spectra were recorded on a Bruker Tensor-27 spectrometer using KBr plate. ^{1}H and ^{13}C NMR spectra were recorded on a Bruker Advance (III) 400 MHz spectrometer. Data for ^{1}H NMR are reported as chemical shift (δ ppm), multiplicity (s = singlet, d = doublet, t = triplet, q = quartet, m = multiplet), coupling constant *J* (Hz), integration, and assignment; data for ^{13}C are reported as chemical shift. High-resolution mass spectral analyses (HRMS) were carried out using ESI-TOF-MS. The absorption spectra were measured at room temperature using a UV-vis Spectrophotometer (Model: Shimadzu UV-1800, Kyoto, Japan) with wavelength accuracy of 0.5 nm. The absorbance (OD) of the solutions at the excited wavelength is 0.1. The absorption spectra were recorded over a range of 200-600 nm. The fluorescence spectra of the molecule were measured using a Fluorescence Spectrophotometer (Model: Hitachi F-2700, Tokyo, Japan) at room temperature with perpendicular geometry. All the theoretical calculations were performed at DFT/B3LYP/6-31G++(d,p) level using Gaussian 09 program.[14] The thermogravimetric analysis (TGA) was carried out using STA7300 Hitachi Thermal Analysis System. The cyclic voltammetric studies were carried out with a computerized Epsilon-2 BAS (Bioanalytical Systems, West Lafayette, USA) potentiostat using a three-electrode systemnamely glassy carbon as working electrode, silver/silver chloride as reference electrode and platinum wire as counter electrode.Melting points were recorded on an Electrothermal melting points apparatus and are uncorrected.

2.2 General synthetic procedure for ethyl 2-(6-aryl-7-oxo-7*H*-furo[2',3':4,5]pyrido[3,2,1-*jk*]carbazol-5-yl)acetate derivatives (3a-h): A mixture

of 4-hydroxy-6*H*-pyrido[3,2,1-*jk*]carbazol-6-one **1** (1.0 mmol mmol), nitroallylic acetates (**2a-h**, 1.2 mmol) and DABCO (1.5 mmol) was magnetically stirred for 12 h in THF (1.5 mL) at room temperature and the reaction was monitored by TLC. After completion of the reaction, the reaction mixture was extracted with ethyl acetate (3×10 mL), washed with water and dried with Na_2SO_4. Afterwards, evaporation of the solvent gave the crude mass which was purified by column chromatography over silica-gel using ethyl acetate/hexane (1:19) as an eluent to afford a pure product. All the synthesized derivatives (**3a-h**) were characterized by their spectroscopic data (IR, ^{1}H, ^{13}C NMR and HRMS).

Ethyl 2-(6-phenyl-7-oxo-7*H*-furo[2′,3′:4,5]pyrido[3,2,1-*jk*]carbazol-5-yl)acetate(3a): Yield 85%; light yellow solid; mp 165-167 ºC; IR (KBr) : ν 1741, 1667, 1551, 1438, 1401, 1333, 1274, 1239, 1151, 1133, 1007 cm^{-1} ; ^{1}H NMR(400 MHz, CDCl$_3$) δ = 8.73 (d, *J* = 7.8 Hz, 1H), 7.95-8.05 (m, 3H), 7.63 (d, *J* = 7.44 Hz, 2H), 7.51 (t, *J* = 7.24 Hz, 4H), 7.42-7.46 (m, 2H), 4.25 (q, *J* = 7.08 Hz, 2H), 3.86 (s, 2H), 1.31 (t, *J* = 7.08 Hz, 3H) ppm ; ^{13}C NMR(100 MHz, CDCl$_3$) δ =168.9, 157.5, 154.9, 147.1, 138.9, 134.2, 130.1, 128.2(2C), 128.1, 126.3, 124.5, 124.2, 123.9, 121.3, 120.7, 118.6, 117.1, 116.7, 110.3, 61.5, 32.9, 14.1 ppm; HRMS (ESI) m/z calcd for $C_{27}H_{20}NO_4$ [M+H]$^+$: 422.1387, found 422.1370.

Ethyl 2-(6-(4-chlorophenyl)-7-oxo-7*H*-furo[2′,3′:4,5]pyrido[3,2,1-*jk*]carbazol-5-yl)acetate (3b): Yield 88%; dark yellow solid; mp 184-186 ºC; IR (KBr): ν 1735, 1690, 1431, 1402, 1381, 1279, 1136, 1054 cm^{-1}; ^{1}H NMR(400 MHz, CDCl$_3$) δ = 8.69 (d, *J* = 8.08 Hz, 1H), 7.98-8.05 (m, 2H), 7.93 (d, *J* = 7.72 Hz, 1H), 7.40-7.58 (m, 7H), 4.25 (q, *J* = 7.08 Hz, 2H), 3.83 (s, 2H), 1.31 (t, *J* = 7.08 Hz, 3H) ppm; ^{13}CNMR(100 MHz, CDCl$_3$) δ =168.8, 157.5, 155.0, 147.3, 138.9, 134.3, 131.5, 129.1, 128.7, 128.5, 128.3, 126.3, 124.7, 124.0, 123.3, 121.5, 120.8, 119.7, 117.1, 116.5, 110.2, 61.7, 32.9, 14.2 ppm; HRMS (ESI) m/z calcd for $C_{27}H_{18}ClNO_4Na$ [M+Na]$^+$: 478.0817, found 478.0817.

Ethyl 2-(6-(4-bromophenyl)-7-oxo-7*H*-furo[2′,3′:4,5]pyrido[3,2,1-*jk*]carbazol-5-yl)acetate (3c): Yield 83%; light yellow solid; mp 185-187 ºC; IR (KBr) : ν 1738, 1684, 1439, 1372, 1277, 1134, 1095 cm^{-1} ; ^{1}H NMR(400 MHz, CDCl$_3$) δ = 8.74 (d, *J* = 8.04 Hz, 1H), 8.12 (d, *J* = 7.52 Hz, 1H), 8.01-8.07 (m, 2H), 7.44-7.64 (m, 7H),

4.24 (q, J = 7.04 Hz, 2H), 3.84 (s, 2H), 1.30 (t, J = 7.04 Hz, 3H) ppm; ^{13}C NMR(100 MHz, CDCl$_3$) δ =168.7, 157.5, 155.0, 147.2,138.9,134.3,132.6,131.7, 131.4, 131.0, 129.1, 128.3, 126.3, 124.7, 124.0, 123.2, 122.5, 121.6, 120.8, 118.7, 117.1, 116.4, 110.2, 61.7, 32.8, 14.1 ppm; HRMS (ESI) m/z calcd for C$_{27}$H$_{18}$BrNO$_4$Na [M+Na]$^+$:522.0311,found 522.0318.

Ethyl 2-(6-(4-methylphenyl)-7-oxo-7*H*-furo[2′,3′:4,5]pyrido[3,2,1-*jk*]carbazol-5-yl)acetate (3d): Yield: 83%; pale yellow solid; mp 170-172 ºC; IR (KBr): ν 1735, 1675, 1441, 1400, 1330, 1283, 1242, 1191, 1129 cm^{-1} ; ^{1}H NMR(400 MHz, CDCl$_3$) δ= 8.76 (d, J = 8.08 Hz, 1H),7.99-8.10 (m, 3H), 7.49-7.60 (m, 4H), 7.42-7.46 (m, 1H),7.30-7.32 (m, 2H),4.24 (q, J = 6.96 Hz, 2H), 3.85 (s, 2H), 2.43 (s, 3H), 1.30 (t, J = 6.96 Hz, 3H) ppm; ^{13}CNMR(100 MHz, CDCl$_3$) δ =169.0, 157.7, 154.9, 147.0, 139.0, 137.8, 134.3, 130.0, 128.9, 128.2, 127.1, 126.4, 124.6, 124.2, 123.9, 121.3, 120.8, 118.7, 117.2, 110.4, 61.5, 32.9, 21.3, 14.1 ppm; HRMS (ESI) m/z calcd for C$_{28}$H$_{21}$NO$_4$Na [M+Na]$^+$:458.1363, found 458.1356.

Ethyl 2-(6-(4-methoxyphenyl)-7-oxo-7*H*-furo[2′,3′:4,5]pyrido[3,2,1-*jk*]carbazol-5-yl)acetate (3e): Yield: 80%; pale yellowish solid; mp 178-180ºC; IR (KBr) : ν 1737, 1679, 1439, 1374, 1131, 1094 cm^{-1} ; ^{1}H NMR(400 MHz, CDCl$_3$) δ = 8.70 (d, J = 8.12 Hz, 1H), 7.95-8.00 (m, 2H), 7.90 (d, J = 7.72 Hz, 1H), 7.56 (d, J = 8.48 Hz, 2H), 7.47-7.51 (m, 2H), 7.38-7.41 (m, 1H), 7.05 (d, J = 8.44 Hz, 2H), 4.26 (q, J = 7.08 Hz, 2H), 3.89 (s, 3H), 3.84 (s, 2H), 1.31 (t, J = 7.08 Hz, 3H) ppm; ^{13}C NMR(100 MHz, CDCl$_3$) δ =169.0, 159.4, 157.6, 154.7, 146.8, 138.8, 134.1, 131.3, 128.0, 126.2, 124.5, 123.9, 123.8, 122.3, 121.2, 120.7, 118.5, 117.0, 116.7, 113.6, 110.0, 61.5, 55.2, 32.9, 14.1 ppm; HRMS (ESI) m/z calcd for C$_{28}$H$_{22}$NO$_5$ [M+H]$^+$: 452.1492, found 452.1472

Ethyl 2-(6-(4-benzyloxy-3-methoxyphenyl)-7-oxo-7*H*-furo[2′,3′:4,5]pyrido[3,2,1-*jk*]carbazol-5-yl)acetate (3f): Yield: 78%; yellow solid; mp 179-181 ºC; **IR** (KBr) : ν1728, 1676, 1442, 1374, 1255, 1130, 1092 cm^{-1} ; ^{1}H NMR(400 MHz, CDCl$_3$) δ = 8.78 (d, J = 7.68 Hz, 1H),8.02-8.13 (m,3H),7.32-7.62 (m, 8H),7.23 (s, 1H),7.12 (d, J = 7.64 Hz, 1H),7.01 (d, J = 7.84 Hz, 1H),5.23(s, 2H),4.23 (d, J = 7.1 Hz, 2H), 3.95 (s, 3H), 3.86 (s, 2H),1.28(t, J =7.1 Hz, 3H) ppm; ^{13}C NMR(100 MHz, CDCl$_3$) δ=169.1,157.7, 154.9, 148.9,148.1, 147.0, 139.0, 137.2, 134.3, 128.5, 128.2, 127.8,

127.2, 126.4, 124.6, 124.1, 124.0, 123.9, 122.9, 122.6, 121.4, 120.8, 118.7, 117.2, 114.0, 113.2, 110.4, 70.9, 61.6, 56.0, 33.0, 14.1ppm;HRMS (ESI) m/z calcd for$C_{35}H_{27}NO_6Na$ [M+Na]$^+$: 580.1731,found 580.1740.

Ethyl 2-(6-(2,5-dimethoxyphenyl)-7-oxo-7H-furo[2′,3′:4,5]pyrido[3,2,1-jk]carbazol-5-yl)acetate (3g): Yield 80%; light yellowish solid; mp 173-175 ℃; IR (KBr) : ν1736, 1680, 1440, 1373, 1131, 1091 cm^{-1} ;^{1}H NMR(400 MHz, CDCl$_3$) δ= 8.69 (d, J = 8.12 Hz, 1H), 7.94-7.99 (m, 2H), 7.89 (d, J = 7.72 Hz, 1H), 7.54-7.56 (m, 2H), 7.46-7.50 (m, 2H), 7.37-7.40 (m, 1H), 7.03-7.05 (m, 1H), 4.25 (q, J = 7.08 Hz, 2H), 3.88 (s, 6H), 3.83 (s, 2H), 1.28-1.32 (m, 3H) ppm; ^{13}C NMR(100 MHz, CDCl$_3$) δ=169.0, 153.1, 151.7, 147.7, 139.0, 134.3, 128.1, 126.4, 124.4, 123.8, 121.2, 120.8, 120.0, 119.9, 118.6, 117.9, 117.5, 117.1, 114.6, 112.2, 110.7, 61.4, 56.2, 55.7, 33.1, 14.1 ppm;HRMS (ESI) m/z calcd for$C_{29}H_{23}NO_6Na$ [M+Na]$^+$: 504.1418, found 504.1418.

Ethyl 2-(6-(2-furyl)-7-oxo-7H-furo[2′,3′:4,5]pyrido[3,2,1-jk]carbazol-5-yl)acetate (3h): Yield 72%; brown solid; mp 160 - 162 ℃; IR (KBr) : ν 1735, 1674, 1441, 1387, 1240, 1128, 1093 cm^{-1} ; ^{1}H NMR(400 MHz, CDCl$_3$) δ = 8.82 (d, J = 8.0 Hz, 1H),8.05-8.11 (m,2H),7.98 (d, J = 7.44 Hz, 1H),7.69 (s, 1H),7.47-7.59 (m, 4H),6.57 (s, 1H),4.20-4.23 (m, 4H), 1.25-1.28 (m, 3H) ppm ; ^{13}C NMR(100 MHz, CDCl$_3$) δ =169.1,157.4, 155.0, 146.9,145.3, 142.0, 138.9, 134.1, 128.2, 126.2, 124.6, 123.9, 123.7, 121.5, 120.8, 118.6, 117.0, 115.2, 114.5, 112.4, 111.6, 109.9, 61.4, 34.5, 14.1 ppm;HRMS (ESI) m/z calcd for$C_{25}H_{17}NO_5Na$[M+Na]$^+$: 434.0999,found 434.0984.

3. Results and discussion

3.1 Synthetic technique

Initially, we carried out a model reaction between HPCO (**1,** 1.0 equiv) with ethyl-2-acetoxy-3-nitro-4-phenylbut-3-enoate (**2a,** 1.2 equiv) in THF solvent using 1.5 equivalent of DABCO as a solid organobase at room temperature for 12 h. Interestingly, a high yield (85%) of **3a** was obtained (Table 1). The formation of **3a** was ascertained by its spectroscopic data (IR, ^{1}H NMR, ^{13}C NMR and HRMS). The FT-IR spectrum of **3a** showed peaks at 1741 and 1667cm^{-1} which correspond to the C=O groups of CO$_2$Et and N-C=O respectively. The ^{1}H NMR(400 MHz,

CDCl$_3$) spectrum displayed the presence of 12 protons in the range of (δ = 7.43-8.73 ppm). A quartet peak at 4.25 with J = 7.08 Hz for two protons is due to the OCH$_2$ of ester. Furthermore, at 3.86 ppm, a singlet peak appears for CH$_2$protons. The triplet peak at 1.31 ppm indicates a methyl group of ester. Similarly, In the ^{13}C NMR(100 MHz, CDCl$_3$) spectrum, total 25 peaks appeared including two carbonyl peaks at 168.9 and 157.5 ppm. In addition, the HRMS data showed the presence of molecular ion peak [M+H]$^+$ at 422.1370 which clearly supports the molecular structure of the desired product **3a**.It is noteworthy to mention that the reaction also proceeded in the absence of base, when DMSO was used as a solvent in the place THF. However, the observed yield of **3a** was only 45% after 48h. By using the above metal-free conditions, several MBH acetates derived from nitroalkenes **(2b-2h)** reacted nicely with **1** to deliver the corresponding fully substituted fused furan derivatives **(3b-h)** in high yields (80-88%, except **3h** for 72%). Notably, various functionalities namely Me, MeO, BnO, Cl, Br, CO$_2$Et, C=O, furan etc were fully intact under present mild conditions.

Table 1. Generality and scope of this annulation reaction for the access to FPCO (**3a-h**)
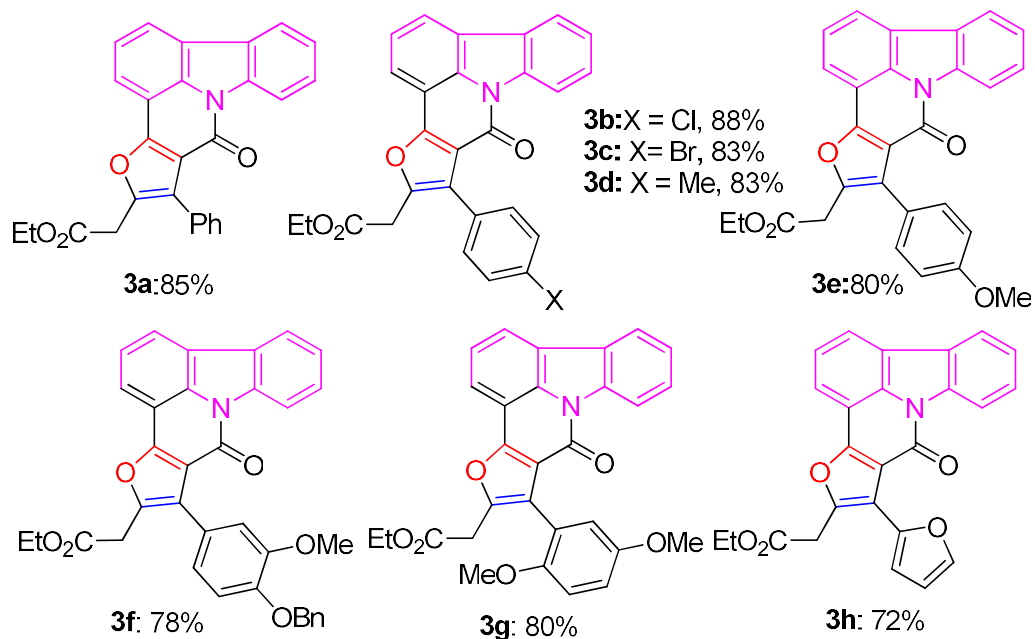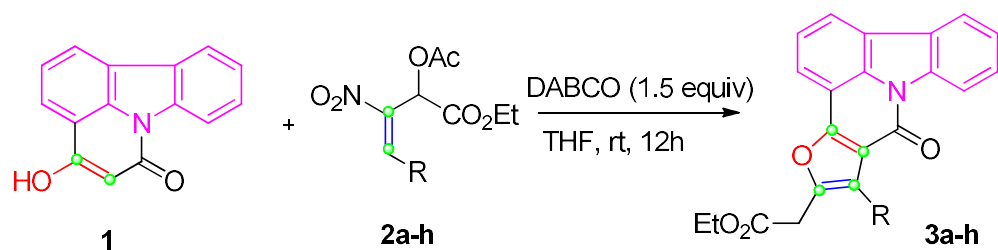
A possible mechanism involves in the formation of **3a** as depicted in Scheme 1. At first, the S_N2' reaction between **1'** (generated in situ from **1** by a base) and **2a** proceeds rapidly to provide an intermediate **4**. It can undergo 5-*exo-trig* cyclization, followed by elimination of HNO_2 to give final product **3a**.
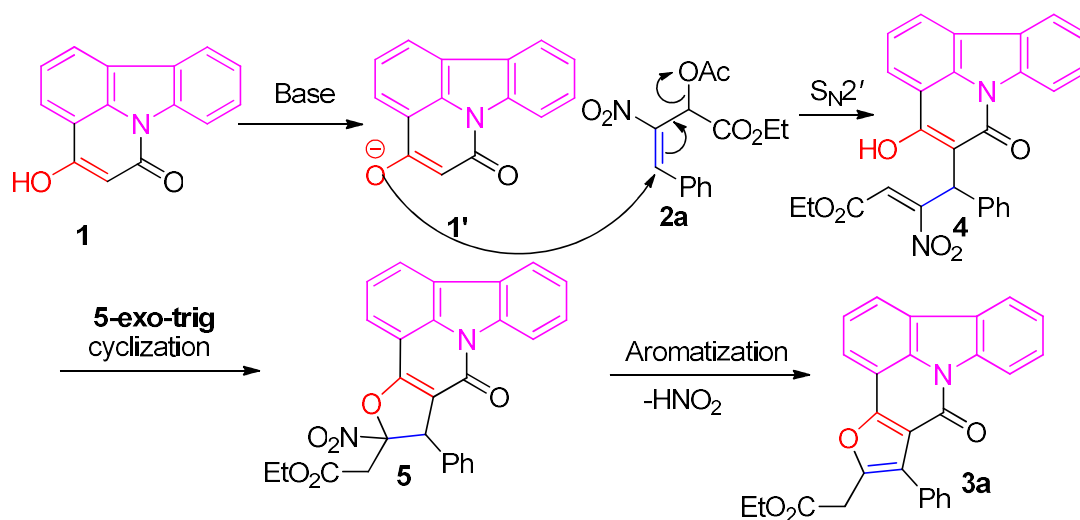
Scheme 1. A plausible mechanism for the formation of **3a**

3.2 Photophysical properties

All the prepared compounds **3a-h** showed blue luminescence under irradiation of UV light which prompted us to evaluate their photophysical studies in detail. At the onset, we recorded absorption spectroscopy of **3a** in various spectroscopic grade solvents such as toluene, xylene, DCM, CHCl$_3$, THF, EtOAc, MeOH and MeCN at room temperature. The results can be seen from Figure 1 and Table 2. The absorption spectra of **3a** exhibit two distinct bands in all the solvents. The shorter wavelength peaks at 349-354 nm are originated from π-π* electronic transition, whereas higher λ_{max} peaks at 367-372 nm correspond to the intramolecular charge transfer (ICT) transition from electron-donor furan unit to PCO moiety. Furthermore, while increasing the polarity of solvents, λ_{max} values have been periodically reduced from 354 to 349 nm (π-π*) and 371 to 367 nm (ICT) (entries 1-8). Therefore, this negative solvatochromism may be attributed due to the solvation, where polar solvent has stabilized the ground state more than excited state. Moreover, FWHM (full width at half maximum) values of **3a** are in general higher at lower λ_{max} than higher ones (17-20 nm vs 12-14 nm). However, molar extinction coefficient (ε) values at higher λ_{max} (20000-62000 mol^{-1} L cm^{-1}) are always more than lower wavelength maxima (17000-45000 mol^{-1}Lcm^{-1}).

Table 2. Photophysical properties of **3a** in different solvents

Entry	Solvent	λ_{max}^a (nm)	FWHM	$\varepsilon \times 10^4$ $(M^{-1}cm^{-1})$	λ_{emi}^b (nm)	Φ^c
1	Toluene	354 371	18 13	4.5 5.8	378 398 422	0.69
2	Xylene	354 372	17 13	2.9 3.4	378 398 421	0.66
3	THF	353 370	19 13	4.5 6.0	376 395 418	0.71
4	DCM	353 370	20 13	3.9 4.4	375 394 417	0.58
5	CHCl$_3$	352 370	20 13	2.7 2.9	374 394 417	0.56
6	EtOAc	351 369	19 12	4.2 6.2	373 393 414	0.61
7	MeCN	350 368	19 14	1.7 2.0	373 393 413	0.40
8	MeOH	349 367	19 13	2.1 2.3	372 392 413	0.43

[a]Absorbance measured in different solvents at 1 x 10^{-5} M concentration. [b]Excitation wavelength at 350 nm. [c]Fluorescence quantum yield was measured by an integrating sphere against quinine sulfate ($\Phi = 0.54$) as a reference at room temperature.ε indicates molar extinction coefficient.
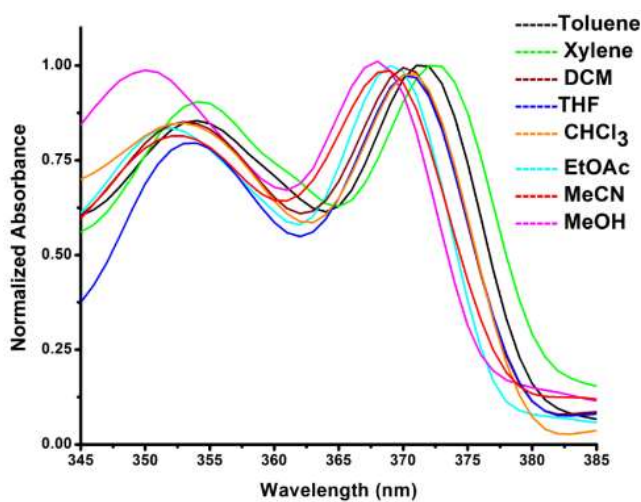
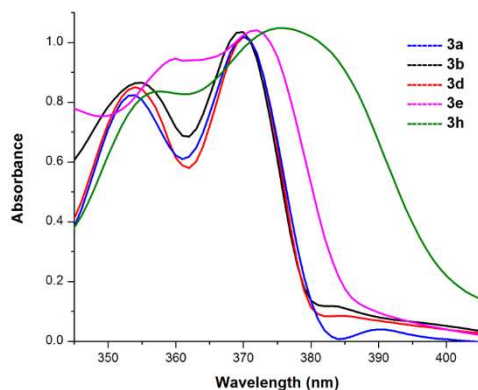**Figure 1**. Solvatochromic effects on absorption spectra of compound **3a** (1×10^{-5} M, 25 °C).

Figure 2. Normalized absorption spectra of compounds **3a-b, 3d-e, 3h** in THF(1×10^{-5} M, 25°C).

The UV-vis spectra of **3b, 3d, 3e** and **3h** were also recorded under identical conditions. Interestingly, compounds **3b** and **3d** exhibited similar absorption bands λ_{max} = 354 nm, 370 nm (FWHM = 17, 14 nm) and λ_{max} = 354 nm, 369 nm (18, 13 nm) with molar extinction coefficients ε of 34000, 48000 $mol^{-1}Lcm^{-1}$ and 36000, 54000 mol^{-1} L cm^{-1} respectively (Table 3, Figure 2). However, the presence of electron-donating moiety appreciably influences the absorption transition property. For example, the compound **3e** having an electron donating anisole moiety absorbed higher wavelengths compared to **3b** (360 nm and 372 nm vs 354 nm and 370 nm, respectively. Furthermore, FWHM values of **3e** are also relatively broader (21 nm, 18 nm), which indicates that compound **3e** has an affinity for strong absorption of light with a wider range of wavelengths. Similarly, **3h** with a furan moiety at C6 position also absorbed nearly 3-6 nm higher wavelengths than **3a** and **3b**. Interestingly, in compound **3h,** due to the large FWHM value (37 nm) at higher λ_{max}, the peak pattern was shown broad along with a high ε value of 65000 $mol^{-1}Lcm^{-1}$. This implies that the furan ring strongly contributes ICT with a large electronic perturbation inside the π-conjugated system.

3.3 Fluorescence properties

The fluorescence spectra of **3a** (Figure 3) were recorded at 350 nm (excitation wavelength) in the above solvents. The relevant photophysical data are summarized in Table 2. All the cases, two clear emission bands at λ_{emi} = 372-378 nm and λ_{emi} = 392-398 nm along with small shoulders at 413-421 nm were observed. Moreover, the emission maxima (λ_{emi}) were gradually blue shifted, while moving from toluene (λ_{emi} = 378, 398 and 422 nm) to MeOH (λ_{emi} = 372, 392 and 413 nm) in tested solvents. Pleasingly, the

11

relative fluorescence quantum yields (Φ) of **3a**were found to be highly emissive in less-polar solvents such as toluene (0.69), xylene (0.66), THF (0.71), DCM (0.58), CHCl₃ (0.56), EtOAc (0.61), whereas quenching of fluorescence was occurred in highly polar solvents like MeOH (0.43) and MeCN (0.40). This may happen due to the freely rotating phenyl group that leads to the twisted ICT state and radiation less relaxation of excited state.[15]

Next, the recorded emission spectra of **3b, 3d, 3e** and **3h** are plotted as shown in Figure 4. The compounds with electron releasing moieties **3d, 3e** and **3h** emit at slightly higher wavelengths (**3d**; λ_{emi} = 376, 396 and 418 nm, **3e**; λ_{emi} = 378, 399 and 423 nm, **3h**; λ_{emi} = 379, 398 and 422 nm) as compared to **3b** (λ_{emi} = 374, 394 and 417 nm). Moreover, electron-donating substituents also tend to ensure higher quantum yieldsin 70-75%, whereas **3b** gives a bit of lower quantum yield in 65% due to the fluorescence quenching by electron withdrawing Cl atom or non-radiative decay of the excited state (Table 3). Notably, all these compounds **3a-b, 3d-e,** and **3h** have shown intense blue fluorescent light.

Table 3. Photophysical properties of compounds **3a-b, 3d-3e** and **3h** in THF.

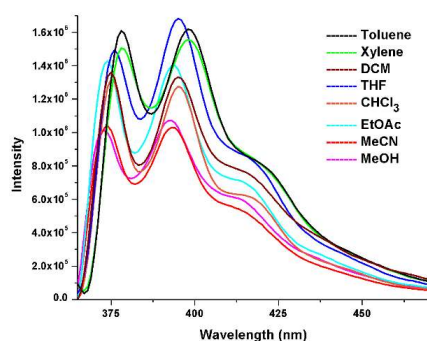| Compound	λ_{abs} (nm)	FWHM (nm)	λ_{emi} (nm)	$\varepsilon \times 10^4$ ($M^{-1}cm^{-1}$)	Φ
3a	353, 370	19, 13	376,395, 418	4.5, 6.0	0.71
3b	354, 370	17, 14	374,394,417	3.4,4.8	0.65
3d	354, 369	18, 13	376,396,418	3.6, 5.4	0.70
3e	360, 372	21, 18	378, 399, 423	4.6, 5.6	0.75
3h	357, 376	21, 37	379,398,422	4.6, 6.5	0.74

Figure 3: Solvatochromic effects on emission spectra of compound **3a** (excited at 350 nm, 25°C, slit = 1/1).
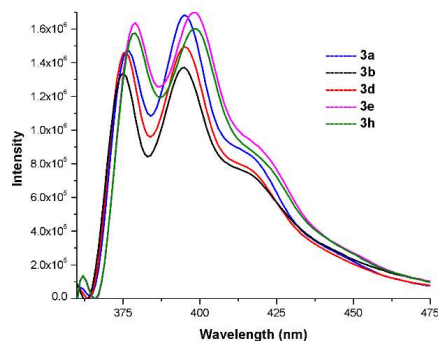
Figure 4: Emission spectra (excited at 350 nm, 25 °C, slit = 1/1) of compounds **3a-b, 3d-e, 3h** in THF

3.4 Theoretical studies

To gain deeper insights of the electronic structure of the fused pentacyclic scaffolds, theoretical calculations were done at DFT/B3LYP/6-311G(d) level of theory using Gaussian 09 program. In this connection, several well-known parameters namely chemical potential (μ), chemical hardness (η) and global softness (s) were calculated for estimating the stability and reactivity associated with the molecular system as summarized in Table 4. Initially, the geometry optimization of **3a** was carried out in various solvents such as toluene, THF, DCM, CHCl$_3$, MeOH and MeCN. Among the solvents, toluene and THF provided a lower HOMO-LUMO energy gap of **3a**. Moreover, the computed energy gap values of **3a** in various solvents are in good correlation with the optical band gap values calculated from absorption spectra (3.21-3.26 eV). The value of chemical hardness η follows the order toluene = THF (η = 1.986) < DCM = CHCl$_3$ (η = 2.000) < MeCN = MeOH (η = 2.013) (Table 4). It means that the tendency of ICT is high in less polar solvents like THF and toluene compared to polar ones. Furthermore, low energy gap (3.973 eV) and high softness (0.2517) indicate less kinetic stability of **3a**. So, **3a** is soft, highly reactive in less polar solvents such as toluene, THF in the comparison to other solvated substrates.[16]

Table 4. Calculated energy and global descriptors for **3a** in different solvents using DFT.

Solvent	HOMO (eV)	LUMO (eV)	TE Gap ΔE (eV)[a]	OB Gap (eV)[b]	μ	η	s	
toluene	-5.959	-1.986	3.973	3.21	-3.973	1.986	0.2517	[a]Theoretical Band Gap calculated from HOM
THF	-6.095	-2.122	3.973	3.22	-4.108	1.986	0.2517	
DCM	-6.068	-2.068	4.000	3.23	-4.068	2.000	0.2499	
CHCl$_3$	-6.040	-2.040	4.000	3.24	-4.040	2.000	0.2499	
MeCN	-6.095	-2.068	4.027	3.25	-4.081	2.013	0.2483	
MeOH	-6.095	-2.068	4.027	3.26	-4.081	2.013	0.2483	

O- LUMO values. [b]Optical Band (OB) Gap calculated from absorption spectra in various solvents.

Next, the molecular descriptors for other compounds **3b**, **3d-e** and **3h** were calculated and tabulated in Table 5. The energy gap follows the order **3e** (3.837 eV) <**3h** (3.919 eV) <**3d** (3.946 eV) <**3b** (4.000 eV) Therefore, the compounds (**3d, 3e** and **3h**) featuring electron-pushing moieties namely anisole, furan and toluene facilitate the electron transfer from donors to acceptors moieties, resulting in lower energy gaps of the corresponding compounds. Moreover, the lower chemical hardness (η = 1.973, 1.918, 1.959, higher chemical potential (μ = -4.068, -4.013 and -4.081 eV), and higher softness values (s= 0.2534, 0.2606, 0.2551) are associated with **3d, 3e** and **3h** which reflect the soft in nature. On the other hand, the presence of electron-withdrawing Cl atom (**3b**) led to the high HOMO-LUMO energy gap (4.000 eV), high chemical hardness (2.000), low softness (0.2500) and low chemical potential value (-4.150). Thus, the molecule **3b** is less polarizable.

Table 5. Calculated energy and global descriptors for **3a-b, 3d-e, 3h** in THF using DFT.

	HOMO (eV)	LUMO (eV)	TE gap ΔE (eV)[a]	OB gap (eV)[b]	μ	η	s
3a	-6.095	-2.122	3.973	3.22	-4.108	1.986	0.2516
3b	-6.150	-2.150	4.000	3.23	-4.150	2.000	0.2500
3d	-6.041	-2.095	3.946	3.22	-4.068	1.973	0.2534
3e	-5.932	-2.095	3.837	3.17	-4.013	1.918	0.2606
3h	-6.041	-2.122	3.919	3.13	-4.081	1.959	0.2551

[a]Theoretical energy (TE) gap calculated from HOMO-LUMO values. [b]Optical band (OB) gap calculated from absorption spectra in various solvents

Next, we began TD-DFT calculations for compound **3a** at B3LYP/6-31G++(d,p) level to explain the electronic transitions in more detail. Various parameters such as transitions, oscillator strengths and composition values are included in Table 6. It was observed that compound **3a** showed two sharp transitions in the visible regions at 319-321 nm and 351-355 nm in all the solvents. It should be noted that the theoretical λ_{max} values are almost 20-30 nm less than experimentally obtained λ_{max} values due to the solvent effects. Furthermore, the computed absorption maxima were gradually blue-shifted from 321 nm (π-π*) to 319 nm (π-π*) and 355 nm (ICT) to 351 nm (ICT), while switching from

toluene (entry 1) to MeOH (entry 6). Therefore, computational results are completely correlated with the solvent effects observed experimentally.

Table 6. The computed absorption maxima (nm and eV), composition and oscillator strength (*f*) for **3a** in various solvents estimated using B3LYP/6-31G++(d,p) level of theory.

Solvent	λ_{abs}^{a} (nm)	λ_{abs}^{b} (nm)	λ_{abs}^{b} (eV)	Composition	*f*
toluene	354	321	3.86	HOMO-1→LUMO (0.64)	0.1420
	371	355	3.48	HOMO→LUMO (0.67)	0.3954
DCM	353	320	3.86	HOMO-1→LUMO (0.65)	0.1568
	370	353	3.51	HOMO→LUMO (0.66)	0.3732
THF	353	320	3.87	HOMO-1→LUMO (0.65)	0.1522
	370	353	3.51	HOMO→LUMO (0.66)	0.3708
CHCl₃	352	320	3.86	HOMO-1→LUMO (0.65)	0.1516
	370	354	3.50	HOMO→LUMO (0.66)	0.3813
MeCN	350	319	3.88	HOMO-1→LUMO (0.64)	0.1523
	368	351	3.52	HOMO→LUMO (0.65)	0.3534
MeOH	349	319	3.88	HOMO-1→LUMO (0.64)	0.1498
	367	351	3.52	HOMO→LUMO (0.65)	0.3506

[a]Absorbance measured in various solvents at 1 x 10^{-5} M concentration.[b] Computed absorption maxima in various solvents.

Inspired by the above results, the compounds **3b, 3d-e** and **3h** have been also calculated in THF, in order to understand the effect of substitution on the absorbance. The computed results are tabulated in Table 7. Expectedly, red-shifts were observed in the following order **3a** (320, 353 nm) <**3b** (321, 352 nm) <**3d** (322, 357 nm) <**3h** (327, 363 nm)<**3e** (329, 368 nm).The frontier molecular orbital (FMO) diagrams at HOMO, LUMO and HOMO-1 levels of **3a-b, 3d-e** and **3h** are depicted in Figure 6. It can be seen from Figure 6 that electron density is majorly located over the fused furan ring at HOMO levels of all the compounds, whereas electron density at LUMO levels is shifted towards the PCO moiety which indicates that the charge transfer occurs from donor furan to acceptor PCO ring. On the other hand, the electronic distribution at HOMO-1 is evenly spread across the whole conjugated system, suggesting π-π* transition from HOMO-1 to LUMO. Thus, π-π* transitions belong to shorter wavelengths with lower oscillator strengths (*f* = 0.1233-0.1610) whereas HOMO→LUMO (ICT) transitions with higher oscillator strengths (*f* = 0.2619-0.3848) are responsible for the longer-wavelengths.

Table 7 Experimental and computational photophysical properties (absorption) for **3a-b, 3d-e, 3h** in THF estimated using B3LYP/6-31G++(d,p) level of theory.

[a]Absorbance measured in THF at 1×10^{-5} M concentration. [b]Computed absorption maxima in THF.

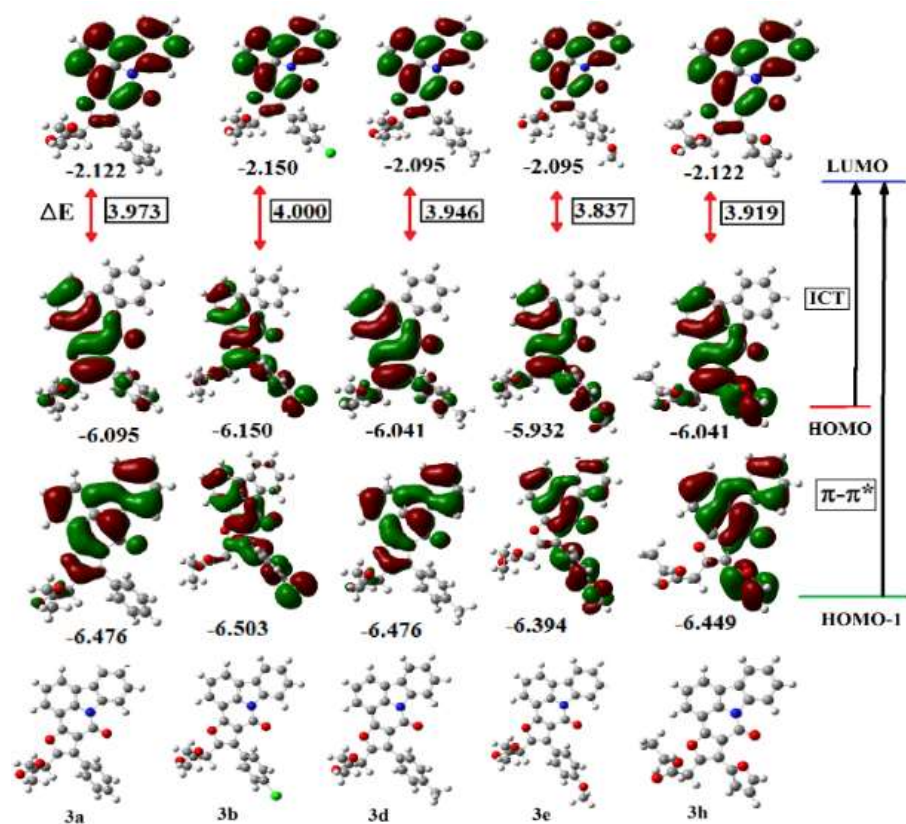|	$\lambda_{abs}{}^{a}$ (nm)	$\lambda_{abs}{}^{b}$ (nm)	$\lambda_{abs}{}^{b}$ (eV)	Composition	f
3a	353	320	3.87	HOMO-1→LUMO (0.65)	0.1522
	370	353	3.51	HOMO→LUMO (0.66)	0.3708
3b	354	321	3.86	HOMO-1→LUMO (0.65)	0.1610
	370	352	3.52	HOMO→LUMO (0.66)	0.3848
3d	354	322	3.84	HOMO-1→LUMO (0.65)	0.1257
	369	357	3.46	HOMO→LUMO (0.67)	0.3562
3e	359	329	3.76	HOMO-1→LUMO (0.60)	0.1362
	371	368	3.36	HOMO→LUMO (0.69)	0.2619
3h	356	327	3.78	HOMO-1→LUMO (0.65)	0.1233
	374	363	3.40	HOMO→LUMO (0.66)	0.2623

Figure 5. The Frontier molecular orbitals of optimized **3a-b, 3d-e, 3h** at B3LYP/6-31G++(d,p) level in THF.

3.5 NBO and surface analysis

In order to predict the reactivity and selectivity, we calculated local reactivity descriptor *i.e.*, Fukui function (f_k) for **3a** using NBO analysis method at DFT/B3LYP/6-31G++(d,p) level. The atom-labelled image for **3a** is depicted in Figure 6. The charge present on each atom was calculated as q_k (k^{th} atom) for cationic (N-1), anionic (N+1) and neutral (N) molecule of **3a**. The atomic sites likely to undergo electrophilic and nucleophilic attack can be ascertained using ω_k and N_k respectively are listed in Table 8. The most nucleophilic sites are O-15, O-16 with N_k values 0.330 and 0.135 respectively whereas most electrophilic sites are C-11, C-12 and C-22 with ω_k values 0.564, 0.360 and 0.420 respectively.
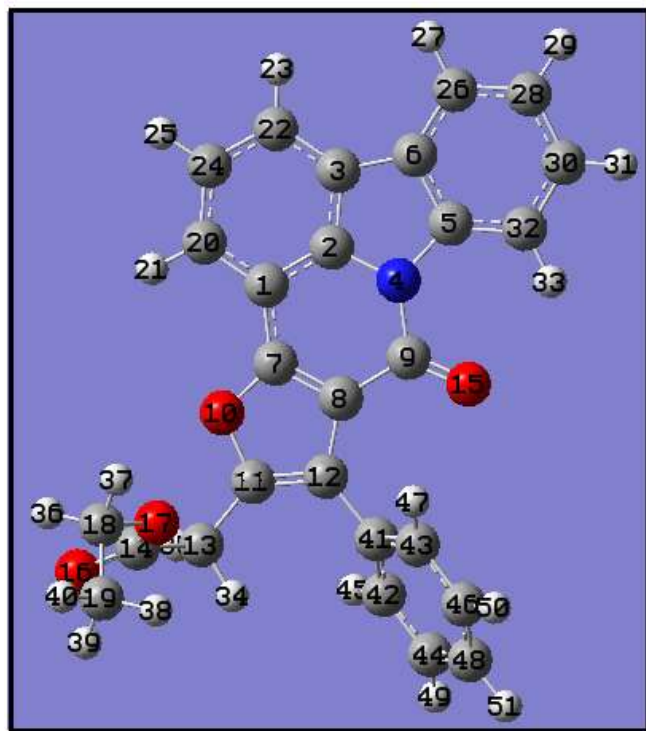
Figure 6. Atom-labelled image of **3a**.

Table 8 Local reactivity descriptors for **3a** in terms of Fukui function using DFT/B3LYP/6-31G++(d,p)level of theory.

Atom	$q_k(N)$	$q_k(N+1)$	f_k+	ω_k
C_1	-0.135	-0.109	0.026	0.104
C_2	0.209	0.257	0.048	0.192
C_3	-0.080	-0.095	-0.015	-0.060
C_5	0.156	0.154	-0.002	-0.008
C_6	-0.083	-0.084	-0.001	-0.004
C_7	0.373	0.405	0.032	0.128
C_8	-0.198	-0.192	0.006	0.024
C_9	0.719	0.712	-0.007	-0.028
C_{11}	0.325	0.466	0.141	0.564
C_{12}	-0.093	-0.003	0.090	0.360
C_{13}	-0.570	-0.603	-0.033	-0.132
C_{14}	0.821	0.831	0.010	0.040
C_{18}	-0.128	-0.113	0.015	0.060
C_{19}	-0.685	-0.694	-0.009	-0.036
C_{20}	-0.199	-0.181	0.018	0.072
C_{22}	-0.137	-0.032	0.105	0.420
C_{24}	-0.272	-0.253	0.019	0.076
C_{26}	-0.211	-0.192	0.019	0.076
C_{28}	-0.248	-0.217	0.031	0.124

	q_k (N)	q_k (N-1)	f_k -	N_k
C$_{30}$	-0.248	-0.208	0.040	0.160
C$_{32}$	-0.190	-0.215	-0.025	-0.100
C$_{41}$	-0.049	-0.065	-0.016	-0.064
C$_{42}$	-0.233	-0.208	0.025	0.100
C$_{43}$	-0.193	-0.165	0.028	0.112
C$_{44}$	-0.239	-0.224	0.015	0.060
C$_{46}$	-0.233	-0.224	0.009	0.036
C$_{48}$	-0.233	-0.167	0.066	0.264
	q_k (N)	q_k (N-1)	f_k -	N_k
N$_4$	-0.425	-0.406	-0.019	-0.064
O$_{10}$	-0.452	-0.442	-0.01	-0.033
O$_{15}$	-0.598	-0.696	0.098	0.330
O$_{16}$	-0.592	-0.632	0.04	0.135
O$_{17}$	-0.564	-0.551	-0.013	-0.043

The molecular electrostatic potential surface diagrams to visualize the reactive sites of all the optimized structures of **3a-b, 3d-e** and **3h** are mapped in Figure 7.The different colours in the maps represent the electrostatic potentials across the surface. Red colour signifies an electronegative region with minimum electrostatic potential, making it susceptible to electrophilic attack. Similarly, blue indicates electropositive suitable for nucleophilic attack and green as a region of zero potential. From the MEP, it is evident that the red region covers the oxygen atom of carbonyl group of pyrido ring and ester, suggesting most reactive towards the intermolecular H-bonding interactions as H-acceptor. On the other hand, hydrogen atoms of carbazole ring and ethyl group are slightly electropositive in nature (blue region).
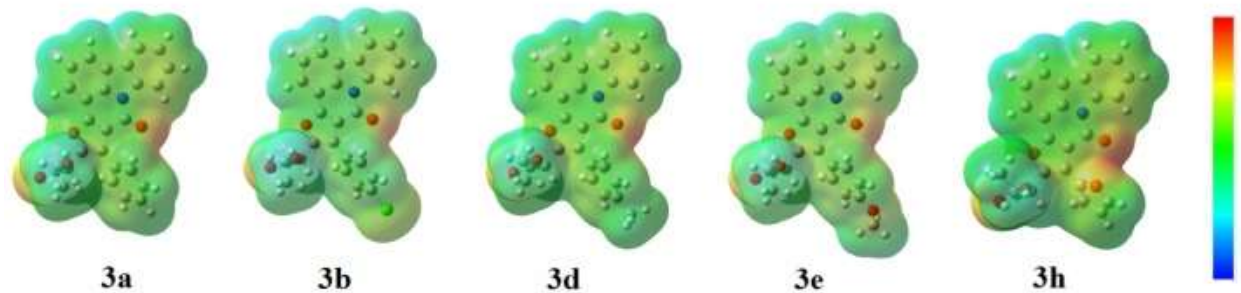

Figure 7. Molecular electrostatic potential (MEP) diagrams of all the compounds.

3.6 Thermal properties

To investigate the degradation behaviours of synthesized FPCO, the thermogravimetric analysis (TGA) of compounds **3a-b, 3d-e** and **3h** was carried out under nitrogen atmosphere at a constant heating rate of 10 °C/min using STA7300 Hitachi Thermal Analysis System. It was observed that the degradation of **3a** has commenced at 337 °C and ended at~415 °C with 50% weight loss (Figure 8). Gratifyingly, the decomposition temperature (T_d)values of other molecules were also very similar such as 339 °C for compound **3b,** 336 °Cfor **3d,** 338 °Cfor **3e** and 335 °C (**3h**). Thus, the newly prepared scaffolds have good thermal stability, hoping for a great possibility for suitable materials.
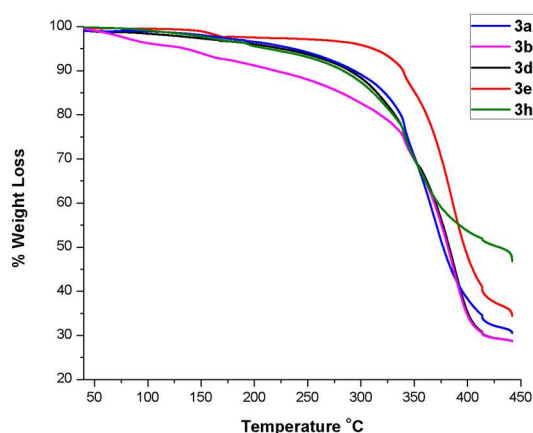

Figure 8. TGA spectra of compounds **3a-b, 3d-e** and **3h.**

3.7Electrochemical properties

The electrochemical studies of compounds **3a-3h** were determined in DMF by using 0.1 M tetrabutylammonium bromide (TBAB) as a supporting electrolyte. Initially, the cyclic voltammograms were collected of **3a** in buffer solution at pH 6.5 ± 0.1 with varying scan rates of 50, 100 and 150 mV/s. In every case, only one irreversible reduction peak was shown irrespective of scan rates. Moreover, the peak potential shifted towards the more negative values with increasing scan rates. The signal-to-noise ratio was maximum at a scan rate of 100 mV/s, thus it was chosen to be the optimum scan rate for analyses of all other compounds. Similarly, using different pH values such as 3.5, 6.5 and 9.5 with fixed scan rate 100 mV/s, the similar kinds of curves were observed (SI). Increase in the value of pH shifted the peak potential towards less negative value which was the indication of

proton participation in the electrode process. Moreover, pH 6.5 was found to be optimal for further studies in terms of better peak shape and stable response. The curve of **3a** shows (Figure 9) a reduction peak at -0.64 V at pH 6.5 with 100 mV/s scan rate. In case of **3e** and **3h,** the CV curves shift slightly more negative reduction potential values at -0.73 V and -0.65 V respectively compared to **3b** -0.62 V. This may be due to the electron donating effect of anisole (**3e**) and furan (**3h**) moieties, making the reduction process easier.
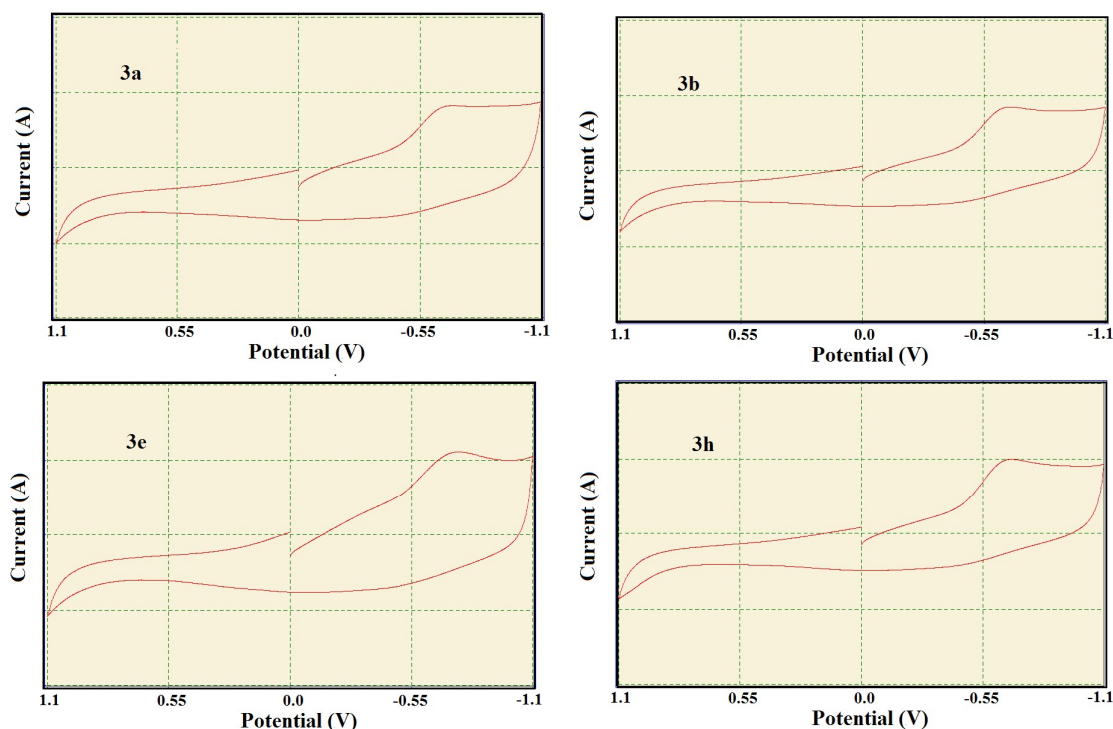

Figure 9. CV curves of **3a, 3b, 3e** and **3h** in DMF at pH 6.5, C= 1x 10^{-5} M.

4.Conclusions

In this paper, we have established a mild (room temperature), efficient, organobase-promoted domino protocol to synthesize highly fluorescent ($\Phi \leq 75\%$) **FPCOs** in good to high yields with good thermal stability (335-339 °C). The molecular structures were fully determined by their spectroscopic data (IR, ^{1}H and 13C NMR, HRMS). These π-extended structural skeletons were shown blue shifts in both absorption and emission spectra upon increasing polarity of solvents. The bathochromic shift is more prominent, when compounds possess electron-donating substituents. DFT and TD-DFT calculations are in good agreement with the experimentally obtained photophysical data that provide the

detailed information of nature of the examined transitions of the above blue emitters. Moreover, various important parameters namely chemical hardness, global softness, chemical potential, local reactivity (i.e. Fukui function) descriptors of compounds were well-estimated. Furthermore, electrochemical studies confirmed the molecules showing irreversible reduction potential values ranging from -0.62 to 0.73V. Based on the significant properties, these donor-acceptor chromophores find potential applications in blue light emitters and optoelectronic materials.

Conflicts of interest

"There are no conflicts to declare".

Credit author statement:MA, SD and AS have synthesized the molecules. MA has performed all the UV-visible and fluorescence spectroscopy, TGA and Electrochemistry studies. MA, PS and AK did theoretical calculations. SShas supervised the findings of this work and written the manuscript.

Competing interest: The authors have declared no competing interest.

References

[1] (a) B. Breiten, I. Biaggio, F. Diederich, Nonplanar push–pull chromophores for opto-electronic applications, Chimia 64 (2010)409-413. (b) Z. I. M. Allaoui, E. l.Gall, A. Fihey, R. Plaza-Pedroche, C. Katan, F. R.-l. Guen,J. Rodríguez-López,S.Achelle, Push–pull

(iso)quinoline chromophores: synthesis, photophysical properties, and use for white-light emission,Chem. Eur. J. 26(2020) 8153-8161. (c) J. M. Hales, S.Barlow, H. Kim, S. Mukhopadhyay, J.-L. Brédas, J. W. Perry,S. R.Marder, Design of organic chromophores for all-optical signal processing applications,Chem. Mater.26 (2014) 549−560. (d) O.Ostroverkhova, organic optoelectronic materials: mechanisms and applications, Chem. Rev.116 (2016) 13279−13412. (e) L. Chen, D.Wu,J.Yoon, Recent advances in the development of chromophore-based chemosensors for nerve agents and phosgene. ACS Sens.3 (2018) 27−43. (f) X. Li, X. Gao, W. Shi,H.Ma, Design strategies for water-soluble small molecular chromogenic and fluorogenic probes , Chem. Rev.114 (2014) 590−659.

[2] (a) J.Zhang, J. Jin, H. Xu, Q. Zhang, W.Huang， Recent progress on organic donor–acceptor complexes as active elements in organic field-effect transistors,J. Mater. Chem. C6 (2018)3485-3498. (b) P. Cusumano, C. Arnone, M. A.Giambra,A.Paris,Donor/Acceptor Heterojunction Organic Solar Cells,Electronics 9 (2020) 70. (c) J. Zhang, W. Xu, P. Sheng, G. Zhao, D. Zhu, Organic Donor–Acceptor Complexes as Novel Organic Semiconductors, Acc. Chem. Res. 50 (2017) 1654−1662. (d) J. Chen, Y. Chen,L.-W. Feng, C. Gu, G. Li,N. Su,G. Wang, S. M. Swick, W. Huang,X. Guo, A. Facchetti, T. J. Marks, Hole (donor) and electron (acceptor) transporting organic semiconductors for bulk-heterojunction solar cells, *EnergyChem*2(2020) 100042.

[3] (a) T. Kojima, I.Kawajiri, J.-I. Nishida, C. Kitamura, H.Kurata,M.Tanaka, H. Ikeda,T. Kawase,2,3-Diphenylphenanthro[9,10-b]furan Derivatives as New Blue Fluorophores,Bull. Chem. Soc. Jpn.89 (2016) 931-940. (b) M. Havlik, V. Talianová, R. Kaplánek, T. Bříza, B. Dolensky, J. Králová, P.Martásek,V. Král, Versatile fluorophores for bioimaging applications: π-expanded naphthalimide derivatives with skeletal and appendage diversity, Chem. Commun.55 (2019)2696-2699. (d) Z.Zhao, H. Nie, C. Ge, Y. Cai, Y. Xiong, J. Qi, W. Wu, R. T. K. Kwok, X.Gao, A. Qin, J. W. Y.Lam,Z. Tang, Furan Is Superior to Thiophene: A Furan-Cored AIEgen with Remarkable Chromism and OLED Performance, Adv. Sci.4 (2017) 1700005. (e) H. Tsuji,E. Nakamura, Design and Functions of Semiconducting Fused Polycyclic Furans for Optoelectronic Applications, Acc. Chem. Res. 50 (2017) 396-406. (f) N. M. Sarih, P. Myers, A. Slater, B. Slater, Z.Abdullah, H. A. Tajuddin, S. Maher, White Light Emission from a Simple Mixture of Fluorescent Organic Compounds,Sci. Rep.9 (2019) 11834.

[4] (a) T. Yanagisawa, N. Bayashi, R. Miyatake, M.Oda, Cyclohepta[*c*]furan-based fluorophores: Synthesis, optical properties, solvatochromism and DFT study, Dyes Pigm.143 (2017)183-189. (b) T.Yanagisawa, K. Kobayashi, R.Miyatake,M.Oda,Synthesis and fluorescence property of 2,3-naphthalimide derivatives bearing phenyl substituents on the naphthalene skeleton, Dyes Pigm136 (2017) 859–864. (c) S. Anderson, P. N. Taylor, G. L. B. Verschoor,Benzofuran Trimers for Organic Electroluminescence,Chem. Eur. J.10 (2004) 518-527. (d) Tsuji, H.; Mitsui, C.;Ilies, L.;Sato,Y.;Nakamura, E.Synthesis and Properties of 2,3,6,7-Tetraarylbenzo[1,2-b:4,5-b']difurans as Hole-Transporting Material,J. Am. Chem. Soc. 129 (2007) 11902-11903. (e) J. Xu, G.Nie, S. Zhang, X. Han, S. Pu,L. Shen,Q. Xiao, Electrosyntheses of poly(2,3-benzofuran) films in boron trifluoride diethyl etherate containing poly(ethylene glycol) oligomers, Euro. Poly. J. 41(2005) 1654-1661.

[5] (a) P. Ledwon, Recent advances of donor-acceptor type carbazole-based molecules for light emitting applications, Org. Electron.75 (2019) 105422. (b) V. V. Patil, K. H.Lee, J. Y. Lee, J. Mater. Chem. C8 (2020) 8320-8327. (c) Y. Yang, Y.Wang, Y. Xie, T. Xiong, Z. Yuan, Y. Zhang, S. Qian,Y.Xiao, Fused perylenebisimide–carbazole: new ladder chromophores with enhanced third-order nonlinear optical activities, Chem. Commun. 47 (2011) 10749-10751. (d) M.-S. Gong, J.-R. Cha, C. W. Lee, Synthesis and device properties of mCP analogues based on fused-ring carbazole moiety, Org. Electron. 42 (2017) 66-77.

[6] (a) A. H. Parham, J. V. Kroeber, J. Engelhart, A. Jatsch, C.Eickhoff, C.Ehrenreich,Materials for organic electroluminescent devices,PCT Int. Appl. (2020) WO 2020016264 A1 20200123. (b) A. Parham, J. Kroeber, C. Ehrenreich, J. Engelhart, C. Eickhoff, J. Pfalzgraf, Matrix materials for emitters in organic electroluminescent devices designed to improve service lifetimeQuick View, PCT Int. Appl. (2020) WO 2020127165 A1 20200625.

[7] Y.-K. Jeong, M.-A.Kim, H.-S. Lee, J.-M. Kim, S. W. Lee,J.-G.Kang, Structural and photophysical properties of HPPCO (4-hydroxy-5-phenyl-6H-pyrido[3,2,1-jk]carbazol-6-one) derivatives, Spectrochim. Acta A Mol. Biomol. Spectrosc.134 (2015)184–190

[8] M. Ahuja, S. Biswas, P. Sharma,S. Samanta, Synthesis and Photophysical Properties of α-Pyrone-fused-pyrido[3, 2,1-jk]carbazolone Derivatives : DFT/TD-DFT Insights, ChemistrySelect 3 (2018) 4354-4360.

[9] (a) W.-Y. Huang, S. Anwar,K. Chen, Morita-Baylis-Hillman (MBH) Reaction Derived Nitroallylic Alcohols, Acetates and Amines as Synthons in Organocatalysis and Heterocycle Synthesis, Chem. Rec.3 (2017) 363-381. (b) V. Mane, T.Kumar, S. Pradhan, S. Katiyar, I. N. N. Namboothiri,One-pot regioselective synthesis of functionalized and fused furans from Morita–Baylis–Hillman and Rauhut–Currier adducts of nitroalkenes, RSC Adv.5 (2015) 69990-69999. (c) Huang,W.-Y.; Chen, Y.-C.; Chen, K. Efficient Synthesis of Tetrasubstituted Furans from Nitroallylic Acetates and 1,3-Dicarbonyl/α-Activating Ketones by Feist–Bénary Addition–Elimination, Chem. Asian J. 7 (2012) 688-691.

[10] (a) M.Ahuja, D. Majee, P. Sharma, A. Kumar, S.M.Mobin, S. Samanta, Metal-Free Based Domino Approach to Pyrano-Fused-Pyrido[3,2,1-*jk*]carbazolones: Antibacterial and Molecular Docking Studies,ChemistrySelect4 (2019) 9096-9101. (b) S. Biswas, D.Majee,A. Dagar, S. Samanta, Metal-Free One-Pot Protocol for the Preparation of Unexpected Carbazole Derivative in Water: Easy Access to Pyrimidocarbazole and Pyridocarbazolone Derivatives, Synlett25 (2014) 2115-2120.

[11] S. Singh, S.Samanta,Efficient One-Pot Access to 2,9-Dihydrothiopyrano[2,3-b]indole Scaffolds Showing Large Stokes Shifts, Chin. J. Chem.33 (2015) 1244-1250.

[12] (a) R. J.Reddy,K. Chen,Highly Efficient Organocatalytic Kinetic Resolution of Activated Nitroallylic Acetates with Aldehydes via Conjugate Addition−Elimination,Org. Lett.13 (2011)1458-1461. (b) I.Deb, P. Shanbhag, S. M. Mobin, I. N. N. Namboothiri, Morita–Baylis–Hillman Reactions Between Conjugated Nitroalkenes or Nitrodienes and Carbonyl Compounds, Eur. J. Org. Chem. (2009) 4091-4101.

[13] W. Stadlbauer, V. H. Dang, N. Guttenberger, 5-Unsubstituted Pyrido[3,2,1-jk]carbazol-6-ones: Syntheses, Substitution, and Cyclization Reactions, J. Heterocycl. Chem.52 (2015) 114-123.

[14] M. J. Frisch, G. W. Trucks, H. B. Schlegel, G. E. Scuseria, M. A. Robb, J. R. Cheeseman, G. Scalmani, V. Barone, G. A. Petersson, H. Nakatsuji, X. Li, M. Caricato, A. Marenich, J. Bloino, B. G. Janesko, R. Gomperts, B. Mennucci, H. P. Hratchian, J. V. Ortiz, A. F. Izmaylov, J. L. Sonnenberg, D. Williams-Young, F. Ding, F.Lipparini, F. Egidi, J.Goings, B. Peng, A. Petrone, T. Henderson, D.Ranasinghe, V. G. Zakrzewski, J. Gao, N.Rega, G. Zheng, W.Liang, M.Hada, M.Ehara, K. Toyota, R. Fukuda, J. Hasegawa, M. Ishida, T. Nakajima, Y. Honda, O. Kitao, H. Nakai, T. Vreven, K. Throssell, J. A. Montgomery, J. E.

Peralta, F. Ogliaro, M.Bearpark, J. J. Heyd, E. Brothers, K. N. Kudin, V. N. Staroverov, T. Keith, R. Kobayashi, J.Normand, K. Raghavachari, A.Rendell, J. C. Burant, S. S. Iyengar, J. Tomasi, M.Cossi, J. M. Millam, M. Klene, C. Adamo, R. Cammi, J. W. Ochterski, R. L. Martin, K. Morokuma, O. Farkas, J. B. Foresman, D. J. Fox, *Gaussian 09,*revision E.01, Gaussian, Inc., Wallingford, CT, USA,2016.

[15]   (a) P. K. Chattaraj, B. Maiti, HSAB Principle Applied to the Time Evolution of Chemical Reactions, J. Am. Chem. Soc. 125 (2003**)** 2705-2710. (b) R. G. Pearson, Chemical hardness and density functional theory, J. Chem. Sci.117 (2005) 369-377.

[16]   M. Karabacak, M.Cinar, FT-IR, FT-Raman, UV spectra and DFT calculations on monomeric and dimeric structure of 2-amino-5-bromobenzoic acid, Spectrochim. Acta, Part A 86 (2012),590-599.